

Experimental Verification of a Computational Real-Time Neuronavigation System for Multichannel Transcranial Magnetic Stimulation



Mohammad Daneshzand, Lucia I. Navarro de Lara, Qinglei Meng,
Sergey Makarov, Işıl Uluç, Jyrki Ahveninen, Tommi Raij,
and Aapo Nummenmaa

1 Introduction

Transcranial Magnetic Stimulation (TMS) is a non-invasive and safe method for activation of cortical regions by delivering high amplitude, short current pulses into a coil adjacent to the subject's scalp. This creates a strong time-varying magnetic field ($\sim 1\text{--}2$ T), which in turn induces an E-field at the surface of the brain [1, 2]. The E-fields can depolarize/hyperpolarize the cell membrane to activate/inhibit neuronal populations [3]. TMS is approved by the FDA for treating neuropsychiatric disorders such as major depressive disorder (MDD) [4] and obsessive-compulsive disorder (OCD) [5], with more clinical applications under investigation. While accurate targeting of a brain region with a single TMS coil is a highly useful and accurate method for various experimental paradigms, characterising the functional connectivity of adjacent areas of a cortical network is only achieved by dual or multichannel TMS systems [6, 7]. Additionally, multichannel TMS arrays allow electronic steering of the induced Electric field (E-field) without the need to physically move the coils [2, 8] resulting in the capability of rapidly shifting the target/focus. This can be accomplished by computationally determining the E-field distribution of each coil in the array individually and then combining them all together to

M. Daneshzand (✉) · L. I. Navarro de Lara · Q. Meng · I. Uluç · J. Ahveninen
T. Raij

Athinoula A. Martinos Center for Biomedical Imaging, Department of Radiology,
Harvard Medical School, Massachusetts General Hospital, Charlestown, MA, USA
e-mail: mdaneshzand@mgh.harvard.edu

S. Makarov
ECE Department, Worcester Polytechnic Institute, Worcester, MA, USA

A. Nummenmaa
Harvard Medical School, Massachusetts General Hospital, Charlestown, MA, USA

synthesize a desired E-field pattern to stimulate any given cortical target according to a user-specified cost-function [2].

In general, a major challenge in TMS targeting is how to position the coil with respect to subject's head for optimal stimulation of a desired brain region [9–11]. To address this, a neuronavigation system can be used in which an optical tracking device localizes the TMS coil with respect to the subject's head [12], ensuring consistent coil placement across multiple TMS sessions [13]. However, using a basic navigation system without anatomically realistic E-field modeling, the actual stimulation intensity at the intracranial target and the surrounding regions remains unknown. Therefore, it is critical to computationally estimate the distribution of the TMS-induced E-field intensity in order to delineate the affected brain regions in real-time [12]. In general, we need to consider several factors for precise computational TMS navigation. First, the anatomy of subject's head must be accurately registered to their MRI data, ensuring that systematic coil positioning errors are minimized [11]. Second, we need to rapidly and accurately calculate the E-field pattern of the TMS coil or coil array to create the best possible “match” with the target area [12]. The real-time E-field based computational neuronavigation is utilized in our multichannel TMS system within a slightly different way such that when the coil array position is fixed with respect to the subject's head, the E-fields need to be computed only once and different current amplitudes will be applied to each coil to synthesize a desired E-field pattern at the target [8]. However, if the subject's head moves between pulses, the currents need to be adjusted to compensate for this, requiring a “near real-time recalculation” of the induced E-fields for all the coils in the array.

For interactive E-field based navigation of the TMS coil during a stimulation session, the E-field distributions need to be ideally computed and displayed within 100 ms (frame rate of 10 Hz). While simple (spherical) models used in commercial neuronavigation systems allow fast E-field computations, they may give inaccurate results due to oversimplification of the volume conductor (head) model [14, 15]. On the other hand, while high resolution individualized head models used in Boundary Element Method (BEM) and Finite Element Method (FEM) reach higher spatial precision, they are computationally too sluggish for real-time navigation requiring ~10 seconds per solution [16–18]. We have previously addressed this speed vs. precision dilemma by introducing a new method based on the concept of an individualized Magnetic Stimulation Profile (MSP) [19]. The real-time E-field estimation by MSP approach leverages pre-calculation of the E-fields from a set of dipoles placed around the head model. The pre-calculations are done with the Boundary Element Method accelerated by the Fast Multipole Method (BEM-FMM) [20, 21]. Since the total E-field of an arbitrary TMS coil only depends on the incident E-field and tissue conductivity boundaries [20], we can find the matching coefficients between the incident E-field of the coil and the dipole basis set approximation, and the total E-field of the coil will be obtained by applying these matching coefficients to the total E-fields of the dipoles [19].

Here we used two 3-axis coils [8] to illustrate how different combinations of the array elements allow steering the E-field ‘hot spot’. Furthermore, our computational multichannel TMS neuronavigation system allows rendering the E-fields of individual 3-axis coils and synthesizing the ‘hot spot’ using the array approach with speed and accuracy suitable for human studies. To verify that the computational neuronavigation system is working as expected, we used two z-elements of our 2×3 -axis coil array connected to individual stimulators to mimic a figure of eight coil to activate the motor cortex and compared the results with a commercially available TMS coil.

This article is organized as follows: In Sect. 2 we describe the design of the 3-axis coils and investigate the efficiency of these coils in a simple 2×3 -axis array configuration by calculating the induced E-field using a spherical model. Section 3 provides a brief description of TMS neuronavigation methods as well as their present limitations in practical applications. In Sect. 4 we briefly describe the methodology behind the MSP approach for real-time calculation of the E-fields and its integration with a commercial TMS navigation system. Finally, in Sect. 5, we demonstrate the efficiency of two z-elements in a 2×3 -axis array in conjunction with the interactive navigation system to elicit Electromyography (EMG) responses in a healthy volunteer.

2 Multichannel TMS Array Design Concept

2.1 *The 3-Axis Coils as the Building Blocks of a TMS Array*

The proposed modular 3-axis multichannel array allows efficient and safe stimulation of any cortical area with high degrees of freedom in shaping and adjusting the orientation of the E-field. Delivering specific current amplitudes for each coil enables simultaneous or sequential stimulation of multiple areas which can be utilized for investigation of causal relationships between cortical areas involved in various information processing tasks [22, 23].

Figure 1a shows the basic conceptual design of our envisioned 48-channel (16×3) TMS array. In this array configuration that has been motivated by our overarching goal of an integrated TMS-compatible MRI acquisition system [24], there are 16 locations for placement of 3-axis coils allowing whole-head coverage. The 3-axis coil consists of three orthogonal circular elements called X, Y and Z as shown in Fig. 1b, c. The goal of this coil design is to achieve high efficiency and focality while offering accurate spatial control of the E-field hot spots using simple coil modules. The purpose of adding the X and Y elements is to cover for the zero E-field at the center of the circular Z-element [8]. Additionally, the X and Y elements will provide more degrees of freedom to the overall field shaping capabilities of the multichannel array. Furthermore, the geometrical design of the X, Y and Z elements eliminates the coupling between them within each unit [8].

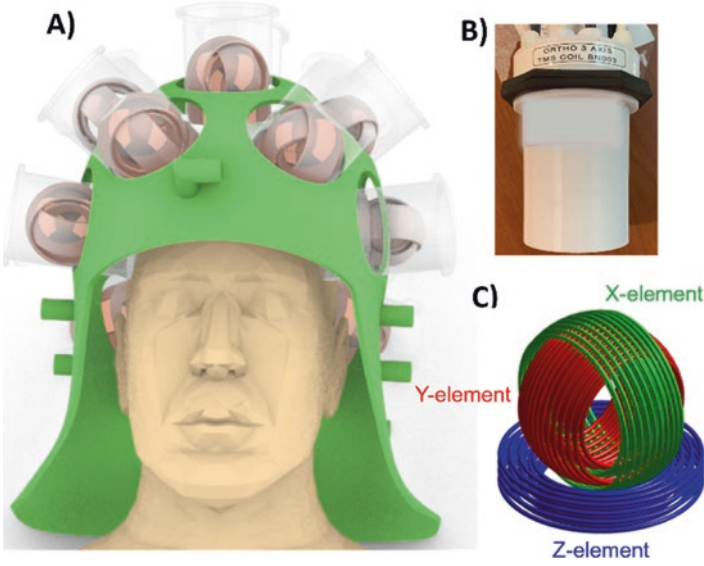


Fig. 1 (a) Multi-channel TMS coil array. (b) prototype of the first of its kind 3-axis coil. (c) Each 3-axis coil consists of three orthogonal elements allowing separate and combined stimulations

2.2 The Numerical Method for E-Field Computation of TMS Coils

The calculation of the E-field induced by each coil element was done using the BEM approach accelerated by the Fast Multipole Method (BEM-FMM) [20]. Based on the Maxwell-Faraday law, the magnetic field of the TMS coil induces an electric field:

$$\nabla \times \mathbf{E} = -\frac{\partial \mathbf{B}}{\partial t}, \quad (1)$$

where B is the magnetic field of the coil. The total electric field \mathbf{E} can be written as:

$$\mathbf{E} = \mathbf{E}^{inc} + \mathbf{E}^s = -\frac{\partial \mathbf{A}}{\partial t} - \nabla \phi \quad (2)$$

The $\mathbf{E}^{inc} = -\partial \mathbf{A} / \partial t$ corresponds to the primary or ‘incident’ field induced by the current in the coil, and the $\mathbf{E}^s = -\nabla \phi$ is called the secondary field that arises from the differences in the electrical conductivities of various tissues inside the head [25]. The BEM-FMM operates with tissue conductivity boundaries where \mathbf{E}^{inc} causes accumulation of surface charges giving rise to the secondary field $-\nabla \phi$. The

boundary integral equations stemming from the quasi-static current conservation conditions $\nabla \cdot \mathbf{J} = \mathbf{0}$ are numerically solved by the Generalized Minimal Residual Method (GMRES) [26]. Once the solution converges and the charge distribution on the conductivity boundaries is known, the total E-field in any region of the 3D space can be obtained.

The individual E-field patterns generated by each element were previously characterized [8] and here we explore different E-field patterns obtained by various combinations of the elements. The coil models were generated in MATLAB [21] (MathWorks, Inc., Natick, MA, USA), placed over a 1-layer spherical model and the E-fields were calculated on the inner sphere at approximately 2 cm distance from the center of the coils. Figure 2 shows the model configuration as well as several calculated E-field patterns based on the activated elements and current polarities. The coil current rate of change $\left(\frac{dI}{dt}\right)$ values were corresponding to 50% of Maximum Stimulator Output (MSO). However, for actual stimulation experiments, the current intensity delivered to each element can be optimized using Minimum Norm Estimate (MNE) method [27] in order to generate a desired E-field pattern.

Figure 2 also shows the E-field pattern of a commercially available figure-of-eight coil (C-B60, MagVenture, Farum, Denmark) as a reference. A similar but somewhat more focal pattern can be generated by combining two of the z-elements (Fig. 2, b8). However, the C-B60 generates a fixed E-field pattern with maximum intensity at the intersection of the two wings and to stimulate a different region the coil must be physically moved. Generally, even a simple multichannel array

Figure 2 also shows the E-field pattern of a commercially available figure-of-eight coil (C-B60, MagVenture, Farum, Denmark) as a reference. A similar but somewhat more focal pattern can be generated by combining two of the z-elements (Fig. 2, b8). However, the C-B60 generates a fixed E-field pattern with maximum intensity at the intersection of the two wings and to stimulate a different region the coil must be physically moved. Generally, even a simple multichannel array

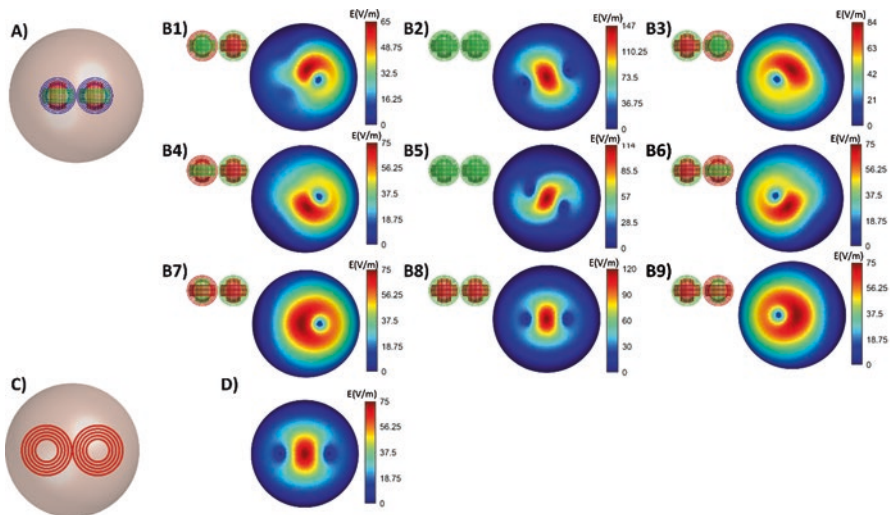


Fig. 2 (a) Two 3-axis coils positioned on a spherical head model. (b1–9) Corresponding E-field distributions of the two 3-axis coils with the activated elements shown in green. (c) A commercially available standard figure-of-eight TMS coil model (MagVenture C-B60) and the corresponding E-field pattern (d)

comprising of two 3-axis coils provides high flexibility in E-field shaping while still offering stimulation intensities comparable to commercially available figure-of-eight coils.

3 TMS Navigation Systems

The rationale of using an image-guided TMS navigation system is to reduce the variability of TMS coil placement with respect to the subject's head and hence to improve the repeatability and accuracy of TMS targeting and dosing [28, 29]. TMS navigator systems typically use optical tracking devices to localize the coil with respect to the subject's head. Anatomical landmarks on the subject's head are identified with corresponding points in the Magnetic Resonance Imaging (MRI) data of the subject, allowing co-registration of the TMS coil position/orientation with the individual anatomy.

Here, we used a commercial TMS neuronavigation system (LOCALITE GmbH, Germany) that employs an optical tracking camera (Polaris Spectra, Northern Digital, Inc. Waterloo, Ontario) to capture the position of the reference and coil trackers and displays the information graphically within the neuronavigation software. Additionally, a specific stimulation target can be defined using the software. The interactive navigation tool allows for accurate positioning of the coil at the target during the stimulation experiment. The positioning of the coil with the neuronavigation system is naturally prone to some errors such as the method used for optical tracking of the coils and the head as well as the registration accuracy of the subject's head to the MR data [30]. Moreover, quantitative high-resolution targeting/dosing of TMS requires knowing the E-field intensity at the desired cortical location and surrounding regions [31] which is necessary especially for multichannel applications but not available on commercial navigation systems. Here, we leveraged our recently developed MSP approach [19] for near real-time TMS E-field calculation combined with a commercial navigation system to track the coil movements and render the induced E-field with a frame rate of 6 Hz.

4 Fast E-Field Calculation with Dipole Based Magnetic Stimulation Profile Approach

A detailed description of the MSP approach can be found in [19]. The computational pipeline of the MSP approach consists of a pre-calculation and a real-time step. In the pre-calculation step, hundreds of magnetic dipoles are distributed uniformly on the scalp model as shown in Fig. 3a, and the incident (field from the dipoles only) and total E-fields (fields from dipoles coil and charge accumulation at tissue conductivity boundaries) are computed using the BEM-FMM method [20]. This fundamental basis solution only needs to be calculated once per subject and can be subsequently used to quickly estimate the E-field created by any TMS coil.

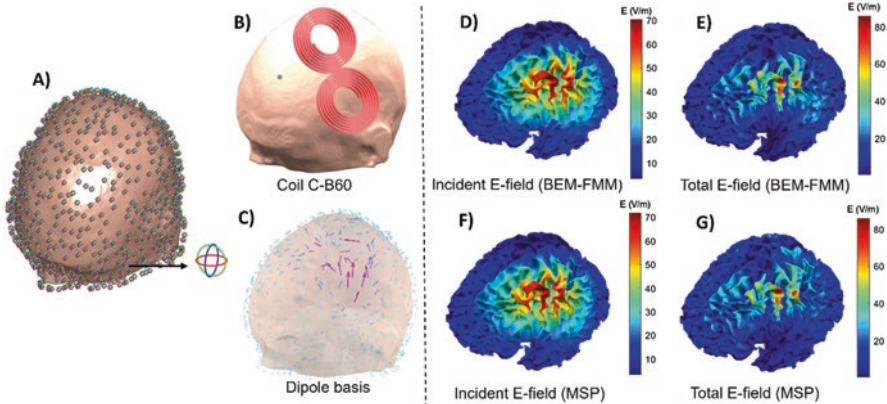


Fig. 3 (a) Spatial configuration of an example basis set with 3 orthogonal magnetic dipoles positioned at several hundreds of locations around the subject’s scalp surface for pre-calculation of the incident and total E-fields. (b) A model of a commercially available TMS coil (C-B60, MagVenture, Farum, Denmark) is placed at an arbitrary location and the dipole amplitudes (c) are optimized to match the incident E-field of the coil. (d, e) the incident and total E-field of the C-B60 coil calculated by the BEM-FMM as the ground truth. (f) The incident E-field obtained from the dipoles basis set. (g) The matching coefficients obtained in (c), are applied to the dipole basis set total E-fields to approximate the total E-field of the coil

The real-time step is based on fundamental physical principles of TMS-induced E-fields:

- The total E-field of a TMS coil only depends on the incident field and the tissue conductivity boundary surfaces and the associated conductivities [1].
- The incident E-field created by the coil in free space can be re-computed very quickly by applying translations/rotations to the set of points where the Incident E-field was initially calculated on.
- By projecting the incident field of the TMS coil onto the set of dipoles and obtaining a set of weights that provide the optimal ‘match’, the same weights can be used to approximate the total E-field based on the principle of superposition [32, 33].

Based on these principles, the pre-calculated E-fields of the dipole basis set can be utilized for a very fast estimation of the total E-field of an arbitrary TMS coil as shown in Fig. 3. This method allows for real-time (100 ms) computational performance and display of the TMS-induced E-field for interactive visualization of the stimulated cortical regions.

Figure 4 shows an example of the real-time setup consisting of a MSP-based computational E-field engine integrated with a commercial navigator system (LOCALITE, Bonn, Germany), using a head phantom. The reference head tracker placed on the phantom allows for co-registration of the head shape with a ‘synthesized MRI dataset’. The position of the coil with respect to phantom is recorded and displayed by the navigator software using the tracker attached to the coil and an optical position measurement camera. The position of the coil(s) (either the two

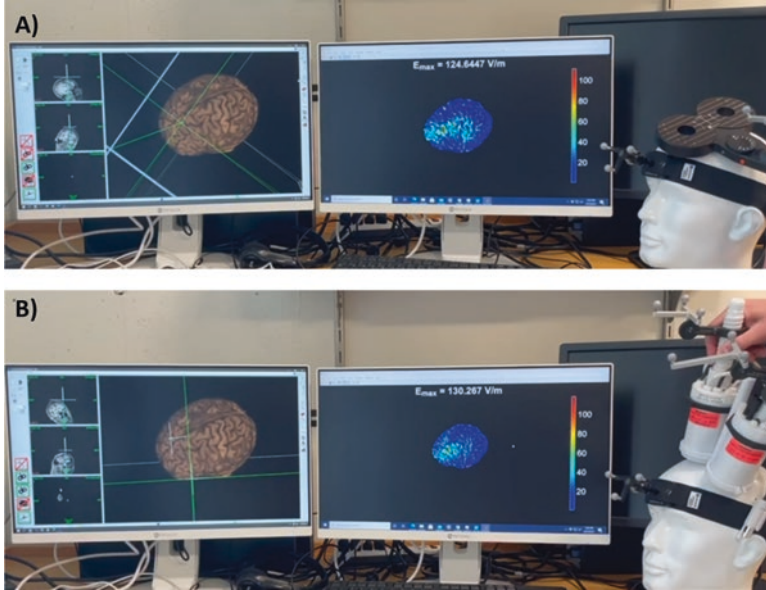


Fig. 4 The real-time E-field computational modeling setup consisting of a commercial neuronavigation system (LOCALITE, Bonn, Germany) interfaced with an external PC for MSP-based calculation and display of (a) a commercial figure-of-eight coil (C-B60) and (b) two custom-made 3-axis coils (Tristan Technologies, San Diego, California)

z-elements of the two 3-axis coils or the C-B60 coil) are then streamed into a second PC using the TCP/IP and JSON protocols implemented in the LOCALITE navigator. Finally, with the coil position/orientation streamed continuously to MATLAB, we can calculate the total E-field and display the results on a cortical surface as shown in Fig. 4. In the current setup, we were able to freely move the coil around the phantom and calculate/visualize the total E-field within a frame rate of 3 Hz and 6 Hz for the two z-elements of the two 3-axis coils and the C-B60 coil, respectively, using MATLAB 2021a on an Intel Xeon(R) Gold 6226R PC with 192 GB of memory.

5 Motor Cortex Stimulation Experiment with Z-Elements of Two 3-Axis Coils

We recruited one healthy male volunteer to evaluate the performance of the simultaneous activation of currents of opposite polarity in the Z-elements of two 3-axis coils in a motor cortex stimulation experiment. Informed consent was obtained from the participant in accordance with the study protocol that was approved by the local IRB at Massachusetts General Hospital. Initially, we acquired the subject's T1-weighted MRI data (1 mm isotropic) on a Siemens Trio 3 T scanner and

reconstructed the tissue compartment boundary surface meshes using the SimNIBS, and Freesurfer tools [34, 35]. The subject’s anatomical landmarks were registered to the MRI data using the Localite neuronavigation system and two separate trackers were mounted on the 3-axis coils to track their position with respect to subject’s head. We set up a TCP/IP protocol to communicate the coordinates of these coils into MATLAB and calculated the combinatory total E-field of the two 3-axis coils. A similar setup was used for the commercial C-B60 TMS coil that was used as a reference.

The EMG data was continuously recorded from the First Dorsolateral interosseous (FDI) muscle of the right hand using the BrainAmp ExG amplifier (Brain Products, Gilching, Germany) and the Motor Evoked Potentials (MEPs) corresponding to each TMS pulse were saved for post-hoc analysis. Either one or two commercially available TMS stimulators were used (MagPro X100, MagVenture) to deliver the current pulses. To identify the FDI MEP hotspot, we started with the stimulation intensity set to 50% MSO and moved the C-B60 TMS coil over the M1 cortex guided with the neuronavigation system with the concurrent display of the E-field similar to the setup described in Fig. 4. Single pulses were delivered, and the intensity was increased until an MEP amplitude of ~50–100 μV was observed. The smallest stimulator output intensity by which the EMG response of at least 50 μV with 50% probability is observed, was then defined as the FDI resting motor threshold (MT) [36]. For quantitative reference, we placed the C-B60 coil at the previously defined FDI ‘hot spot’ and recorded the MT as well as several clearly suprathreshold MEPs (at 107% resting MT). Next, the 2x3-axis coil array was positioned over the FDI hot spot and the z-elements of the two 3-axis coils were synchronously activated to mimic a figure-of-eight coil configuration. The stimulation intensity was increased until clearly suprathreshold MEPs were observed. The post-hoc analysis of the MEP responses in Fig. 5 shows that both dual z-elements and the

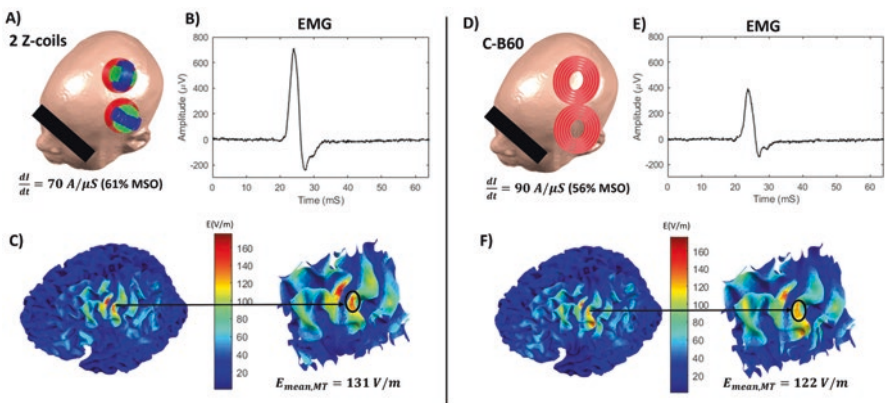


Fig. 5 (a) The z-elements of two 3-axis coils stimulating the left M1 hand area. (b) The recorded MEPs from FDI muscle. (c) The E-field distribution on the white matter surface. (d, e) Corresponding results for the C-B60 coil

C-B60 coil elicited suprathreshold responses with similar EMG morphologies recorded at the FDI muscle. Furthermore, the computationally estimated cortical E-fields show robust agreement for both the amplitudes and the spatial patterns.

6 Summary and Discussion

A key requirement of multi-channel TMS technology is fast and accurate computation of the E-fields from all coil elements to determine the optimal linear combination of the input current values in order to stimulate a desired cortical target region. In this study, we demonstrated that precise and fast computation of the E-field can be achieved by (1) reconstructing high resolution surfaces meshes based on the individual MRI data, (2) reducing the computational burden of high resolution E-field modeling by leveraging the MSP-based approach utilizing a spatially fixed dipole basis set, and (3) retrieving the pre-calculated solutions for the near-real time step to obtain the total E-field by means of simple matrix multiplications based on matching the incident field of the TMS coil with the dipole basis set [19]. The position of the TMS coils with respect to subject's head can be acquired with an optical tracking camera and displayed in a neuronavigation software with frame rates of 10–15 Hz. This gives us a time frame of 60–100 ms for E-field calculations to be performed for an interactive navigation pipeline. Our results suggest that we are able to calculate the E-field of a C-B60 coil within this timeframe on a high-resolution WM surface with about 100 K triangular mesh elements. For the multi-channel TMS arrays the E-field computation time will increase based on the number of coils and coil elements used. However, we plan to improve the computational efficiency further by utilizing a parallel computation approach to obtain the E-field of each coil in the array.

Additionally, we showed that the z-elements of the two 3-axis coils are capable of clearly suprathreshold stimulation when used in a 'dual-channel array' driven by synchronized triggering of two independent TMS stimulators. For more flexible stimulation, the orthogonal placement of the elements in the 3-axis coil provides efficient decoupling between the elements while granting three degrees of freedom in shaping the induced E-field pattern. Moreover, arranging several 3-axis coils in an array will further increase the degrees of freedom for efficient stimulation of a target area with a desired field orientation without the need for physical movement of the coils. We have recently developed a novel 9-channel stimulator system in partnership by MagVenture, by which each element of the 3-axis coils can be driven by independent stimulator units, allowing delivery of pulses with high combined power.

The experimental results show that the juxtaposition of two Z-elements provides an E-field intensity and spatial distribution similar to the commercially available C-B60 coil, producing clear suprathreshold stimulation as measured with MEPs. Furthermore, the MSP-approach used in multi-channel TMS array can be used as a pre-planning step to rapidly calculate the E-field at several locations based on

specific criteria of the experiment [37] or to optimize the positions/orientations of the individual 3-axis coil elements. The biophysical signals recorded during the experiment can also be paired with the previously calculated E-field patterns for post-hoc analysis [38, 39], or be utilized as feedbacks to adjust the stimulation parameters (*e.g.*, input current to each coil) in a closed-loop stimulation paradigm [40–42].

Acknowledgements The research was supported by NIH R01MH11829, P41EB030006, and R01DC016915.

References

1. B.J. Roth, L.G. Cohen, M. Hallett, W. Friauf, P.J. Basser, A theoretical calculation of the electric field induced by magnetic stimulation of a peripheral nerve. *Muscle Nerve* **13**(8), 734–741 (1990). <https://doi.org/10.1002/mus.880130812>
2. J. Ruohonen, R.J. Ilmoniemi, Focusing and targeting of magnetic brain stimulation using multiple coils. *Med. Biol. Eng. Comput.* **36**(3), 297–301 (1998)
3. F. Rattay, The basic mechanism for the electrical stimulation of the nervous system. *Neuroscience* **89**(2), 335–346 (1999)
4. J.P. O’Reardon et al., Efficacy and safety of transcranial magnetic stimulation in the acute treatment of major depression: a multisite randomized controlled trial. *Biol. Psychiatry* **62**(11), 1208–1216 (2007). <https://doi.org/10.1016/j.biopsych.2007.01.018>
5. L. Carmi et al., Efficacy and safety of deep transcranial magnetic stimulation for obsessive-compulsive disorder: a prospective multicenter randomized double-blind placebo-controlled trial. *Am. J. Psychiatry* **176**(11), 931–938 (2019). <https://doi.org/10.1176/appi.ajp.2019.18101180>
6. S. Groppa, N. Werner-Petroll, A. Münchau, G. Deuschl, M.F.S. Ruschworth, H.R. Siebner, A novel dual-site transcranial magnetic stimulation paradigm to probe fast facilitatory inputs from ipsilateral dorsal premotor cortex to primary motor cortex. *NeuroImage* **62**(1), 500–509 (2012). <https://doi.org/10.1016/j.neuroimage.2012.05.023>
7. Y. Roth, Y. Levkovitz, G.S. Pell, M. Ankry, A. Zangen, Safety and characterization of a novel multi-channel TMS stimulator. *Brain Stimul.* **7**(2), 194–205 (2014). <https://doi.org/10.1016/j.brs.2013.09.004>
8. L.I.N. de Lara et al., A 3-axis coil design for multichannel TMS arrays. *NeuroImage* **224**, 117355 (2020)
9. L.D. Gugino et al., Transcranial magnetic stimulation coregistered with MRI: a comparison of a guided versus blind stimulation technique and its effect on evoked compound muscle action potentials. *Clin. Neurophysiol.* **112**(10), 1781–1792 (2001)
10. T. Picht, J. Schulz, M. Hanna, S. Schmidt, O. Suess, P. Vajkoczy, Assessment of the influence of navigated transcranial magnetic stimulation on surgical planning for tumors in or near the motor cortex. *Neurosurgery* **70**(5), 1248–1257 (2012)
11. R. Sparing, D. Buelte, I.G. Meister, T. Pauš, G.R. Fink, Transcranial magnetic stimulation and the challenge of coil placement: a comparison of conventional and stereotaxic neuronavigational strategies. *Hum. Brain Mapp.* **29**(1), 82–96 (2008)
12. J. Ruohonen, J. Karhu, Navigated transcranial magnetic stimulation. *Neurophysiol. Clin. Neurophysiol.* **40**(1), 7–17 (2010)
13. U. Herwig et al., The navigation of transcranial magnetic stimulation. *Psychiatry Res. Neuroimaging* **108**(2), 123–131 (2001)

14. L. Heller, D.B. van Hulsteyn, Brain stimulation using electromagnetic sources: theoretical aspects. *Biophys. J.* **63**(1), 129–138 (1992)
15. A. Nummenmaa, M. Stenroos, R.J. Ilmoniemi, Y.C. Okada, M.S. Hämäläinen, T. Raij, Comparison of spherical and realistically shaped boundary element head models for transcranial magnetic stimulation navigation. *Clin. Neurophysiol. Off. J. Int. Fed. Clin. Neurophysiol.* **124**(10), 1995–2007 (2013). <https://doi.org/10.1016/j.clinph.2013.04.019>
16. F.S. Salinas, J.L. Lancaster, P.T. Fox, 3D modeling of the total electric field induced by transcranial magnetic stimulation using the boundary element method. *Phys. Med. Biol.* **54**(12), 3631 (2009)
17. A. Opitz, M. Windhoff, R.M. Heidemann, R. Turner, A. Thielscher, How the brain tissue shapes the electric field induced by transcranial magnetic stimulation. *NeuroImage* **58**(3), 849–859 (2011)
18. I. Laakso, A. Hirata, Fast multigrid-based computation of the induced electric field for transcranial magnetic stimulation. *Phys. Med. Biol.* **57**(23), 7753–7765 (2012). <https://doi.org/10.1088/0031-9155/57/23/7753>
19. M. Daneshzand, S. N. Makarov, L. I. Navarro de Lara, B. Guerin, J. McNab, B. R. Rosen, M. S. Hämäläinen, T. Raij, and A. Nummenmaa, Rapid computation of TMS-induced E-fields using a dipole-based magnetic stimulation profile approach. *NeuroImage* **237**(2021)
20. S.N. Makarov, G.M. Noetscher, T. Raij, A. Nummenmaa, A quasi-static boundary element approach with fast multipole acceleration for high-resolution bioelectromagnetic models. *I.E.E.E. Trans. Biomed. Eng.* **65**(12), 2675–2683 (2018)
21. S.N. Makarov, W.A. Wartman, M. Daneshzand, K. Fujimoto, T. Raij, A. Nummenmaa, A software toolkit for TMS electric-field modeling with boundary element fast multipole method: an efficient MATLAB implementation. *J. Neural Eng.* (2020). <https://doi.org/10.1088/1741-2552/ab85b3>
22. K. Davranche, C. Tandonnet, B. Burle, C. Meynier, F. Vidal, T. Hasbroucq, The dual nature of time preparation: neural activation and suppression revealed by transcranial magnetic stimulation of the motor cortex. *Eur. J. Neurosci.* **25**(12), 3766–3774 (2007)
23. F. Ferreri, P.M. Rossini, TMS and TMS-EEG techniques in the study of the excitability, connectivity, and plasticity of the human motor cortex. *Rev. Neurosci.* **24**(4), 431–442 (2013)
24. L.I. de Lara, L. Golestanirad, S.N. Makarov, J.P. Stockmann, L.L. Wald, A. Nummenmaa, Evaluation of RF interactions between a 3T birdcage transmit coil and transcranial magnetic stimulation coils using a realistically shaped head phantom. *Magn. Reson. Med.* **84**(2), 1061–1075 (2020)
25. P.C. Miranda, L. Correia, R. Salvador, P.J. Basser, Tissue heterogeneity as a mechanism for localized neural stimulation by applied electric fields. *Phys. Med. Biol.* **52**(18), 5603–5617 (2007). <https://doi.org/10.1088/0031-9155/52/18/009>
26. Y. Saad, M.H. Schultz, GMRES: A generalized minimal residual algorithm for solving non-symmetric linear systems. *SIAM J. Sci. Stat. Comput.* **7**(3), 856–869 (1986)
27. M.S. Hämäläinen, R.J. Ilmoniemi, Interpreting magnetic fields of the brain: minimum norm estimates. *Med. Biol. Eng. Comput.* **32**(1), 35–42 (1994). <https://doi.org/10.1007/BF02512476>
28. A.T. Sack, R.C. Kadosh, T. Schuhmann, M. Moerel, V. Walsh, R. Goebel, Optimizing functional accuracy of TMS in cognitive studies: a comparison of methods. *J. Cogn. Neurosci.* **21**(2), 207–221 (2009)
29. B. Langguth, T. Kleinjung, M. Landgrebe, D. De Ridder, G. Hajak, rTMS for the treatment of tinnitus: the role of neuronavigation for coil positioning. *Neurophysiol. Clin. Neurophysiol.* **40**(1), 45–58 (2010)
30. J. Ruohonen, J. Karhu, Navigated transcranial magnetic stimulation. *Neurophysiol. Clin.* **40**(1), 7–17 (2010). <https://doi.org/10.1016/j.neucli.2010.01.006>
31. N. Sollmann et al., Comparison between electric-field-navigated and line-navigated TMS for cortical motor mapping in patients with brain tumors. *Acta Neurochir.* **158**(12), 2277–2289 (2016)

32. B.B. Baker, E.T. Copson, *The Mathematical Theory of Huygens' Principle*, vol 329 (AMS Chelsea Publishing, Providence, Rhode Island, 2003)
33. L.M. Koponen, J.O. Nieminen, R.J. Ilmoniemi, Minimum-energy coils for transcranial magnetic stimulation: application to focal stimulation. *Brain Stimul.* **8**(1), 124–134 (2015). <https://doi.org/10.1016/j.brs.2014.10.002>
34. A. Thielscher, A. Antunes, G.B. Saturnino, Field modeling for transcranial magnetic stimulation: a useful tool to understand the physiological effects of TMS?, in *2015 37th annual international conference of the IEEE engineering in medicine and biology society (EMBC)*, 2015, pp. 222–225
35. B. Fischl, FreeSurfer. *NeuroImage* **62**(2), 774–781 (2012)
36. S. Rossi, M. Hallett, P.M. Rossini, A. Pascual-Leone, Safety, ethical considerations, and application guidelines for the use of transcranial magnetic stimulation in clinical practice and research. *Clin. Neurophysiol. Off. J. Int. Fed. Clin. Neurophysiol.* **120**(12), 2008–2039 (2009). <https://doi.org/10.1016/j.clinph.2009.08.016>
37. A. Nummenmaa et al., Targeting of white matter tracts with transcranial magnetic stimulation. *Brain Stimul.* **7**(1), 80–84 (2014)
38. J. Ahveninen et al., Evidence for distinct human auditory cortex regions for sound location versus identity processing. *Nat. Commun.* **4**(1), 1–8 (2013)
39. T. Raij et al., Prefrontal cortex stimulation enhances fear extinction memory in humans. *Biol. Psychiatry* **84**(2), 129–137 (2018)
40. D. Kraus et al., Brain state-dependent transcranial magnetic closed-loop stimulation controlled by sensorimotor desynchronization induces robust increase of corticospinal excitability. *Brain Stimul.* **9**(3), 415–424 (2016)
41. J. Meincke, M. Hewitt, G. Batsikadze, D. Liebetanz, Automated TMS hotspot-hunting using a closed loop threshold-based algorithm. *NeuroImage* **124**, 509–517 (2016)
42. T.O. Bergmann et al., EEG-guided transcranial magnetic stimulation reveals rapid shifts in motor cortical excitability during the human sleep slow oscillation. *J. Neurosci.* **32**(1), 243–253 (2012)

Open Access This chapter is licensed under the terms of the Creative Commons Attribution 4.0 International License (<http://creativecommons.org/licenses/by/4.0/>), which permits use, sharing, adaptation, distribution and reproduction in any medium or format, as long as you give appropriate credit to the original author(s) and the source, provide a link to the Creative Commons license and indicate if changes were made.

The images or other third party material in this chapter are included in the chapter's Creative Commons license, unless indicated otherwise in a credit line to the material. If material is not included in the chapter's Creative Commons license and your intended use is not permitted by statutory regulation or exceeds the permitted use, you will need to obtain permission directly from the copyright holder.

